Received: 4 September 2020 | Revised: 16 January 2021 | Accepted: 17 March 2021

IET Electric Power Applications

DOI: 10.1049/elp2.12082

The Institution of Engineering and Technology WILEY

ORIGINAL RESEARCH PAPER

# Unaligned inductance calculation using flux tube approach for rotor conducting screen-based SRM

Aly A. Abdel-Aziz[1] | Khaled H. Ahmed[1,2] | Ahmed M. Massoud[3] | Barry W. Williams[1]

[1]Department of Electronic and Electrical Engineering, University of Strathclyde, Glasgow, UK

[2]Department of Electrical Engineering, Faculty of Engineering, Alexandria University, Alexandria, Egypt

[3]Department of Electrical Engineering, College of Engineering, Qatar University, Doha, Qatar

**Correspondence**

Ahmed M. Massoud, Department of Electrical Engineering, College of Engineering, Qatar University, Doha, 2713, Qatar.
Email: ahmed.massoud@qu.edu.qa

**Funding information**

Qatar National Library

**Abstract**

This article investigates the effect of utilising rotor conducting screens within a switched reluctance machine (SRM). Conducting, non-magnetic materials such as aluminium or copper are inserted into the interpole regions of the rotor. The effective unaligned inductance decreases, which increases the conversion area allowing the machine to develop more power. Predicting machine performance implies knowing the value of the unaligned inductance. A procedure for calculating the effective unaligned inductance for screened motors using the flux tube method is presented. Finite element analysis results establish the validity of the proposed calculation method. A detailed design procedure for screened SRM is presented.

## 1 | INTRODUCTION

Despite the salient advantages of switched reluctance machine (SRM) such as simple and rigid construction, fault-tolerant capability, and wide constant power range, it suffers from low power density when compared with an equivalent-sized permanent magnet synchronous machine (PMSM) [1].

The concept of conducting screens was proposed in [2] to increase the output torque. Conducting, non-magnetic materials such as aluminium or copper are inserted in the interpole regions of the rotor. The conducting screens encounter a time-varying flux due to motor rotation, which induces a voltage. The induced voltage produces eddy currents, which in turn produce flux that opposes the original stator pole flux. The opposing flux results in a decrease in the effective unaligned inductance. In [3–5], the rotor conducting screens were tested for four-phase (8/6), two-phase (4/2), and single-phase (2/2) SRM, respectively.

It is time consuming to use finite element analysis (FEA) to predict motor performance in the early design stage [6]. Any change in the motor geometrical dimensions, number of stator/rotor poles, turns number, excitation current, or firing angles dictate a new model to be built and simulated, involving a time-consuming process. Thus, suitable analytical methods can provide a compromise between accuracy and speed of calculation [7]. To predict motor performance, the unaligned inductance should be known. There was no attempt to calculate the effective unaligned inductance for an SRM with conducting screens in the available literature.

A detailed calculation method based on flux tubes is presented here [8] to calculate the effective unaligned inductance for screened SRM. The proposed method is validated by the FEA using four different SRMs.

The article contribution is summarised as follows:

- A calculation method is proposed to calculate the effective unaligned inductance for screened SRM.
- Linear magnetic equivalent circuit (MEC) for screened SRM is proposed.
- The proposed MEC does not require any iterative solution as opposed to the conventional methods.
- A detailed design method is presented for SRM with rotor conducting screens.

The article is organised as follows. Section 2 gives a brief insight into the salient features of the SRM with rotor

conducting screens. Section 3 presents a detailed derivation for calculating the effective unaligned inductance for screened SRM using the flux tube method. 2D and 3D FEA results are presented in section 4 to validate the proposed method. A detailed design procedure for screened SRM is presented in section 5. Finally, an insight into noise and torque ripple minimisation is presented in section 6.

## 2 | SRM WITH ROTOR CONDUCTING SCREENS

In simplistic terms, the current into an SRM (at phase current turn-on) can be expressed by

$$V = L\frac{di}{dt} \tag{1}$$

The objective is to force the current into the machine as quickly as possible, that is, through maximising the $di/dt$ term, the base-speed, whence the output power can be increased. The inductive term $L$ is related to the machine design, and specifically low $L$ (for $V$ fixed) at only phase turn-on which increases the conversion area, as shown in Figure 1, and hence increase the output power (higher $L$ is required at the turn-off to maximise the machine co-energy).

Moreover, torque is dependent on the area enclosed between the flux linkage $\lambda$ and current $i$ (which represents the increase in co-energy when the rotor moves from unaligned to aligned position). Increasing this difference produces more torque and hence output power, as shown in Figure 1. Equation (2) defines the maximum average torque:

$$T_{av} = \frac{Area\ OAB}{4\pi} N_s N_r \tag{2}$$

where $N_s$ and $N_r$ represent the number of stator and rotor poles, respectively.

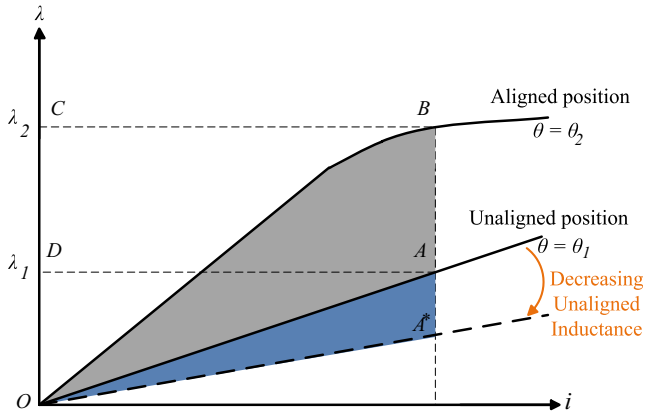


**FIGURE 1** Flux linkage-current ($\lambda$–$i$) characteristics

To decrease the unaligned inductance (without affecting the aligned performance), the spaces between rotor poles can be filled with non-magnetic, electrically conducting materials such as aluminium or copper, as shown in Figure 2; this material is referred to as the conducting screen. The conducting screens are electrically isolated from the rotor, and there is no electrical connection between the conducting screens.

Due to motor rotation along with stator coil excitation, the conducting screens encounter a time-varying flux, which in turn induces voltage ($V \propto d\varphi/dt$).

The induced voltage produces circulating eddy currents that produce flux ($i \propto \varphi$). The produced flux opposes the original flux from the stator poles. The opposing flux (which increases the effective flux air path length and reduces the effective area) results in a decrease in the effective unaligned inductance allowing rapid current building up at initial winding excitation, as demonstrated in Figure 3, which increases the motor output torque.

To gain insight into the effect of rotor conducting screens on the SRM performance, Figure 4a,b show the flux path for unscreened and screened SRMs, respectively, when one stator phase is excited. Figure 4b shows that the reaction field produced by the eddy current in the copper screen opposes the stator magnetic field, hence preventing the flux lines from

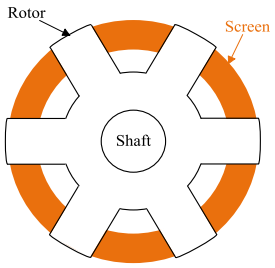


**FIGURE 2** Rotor conducting screens in the interpole regions

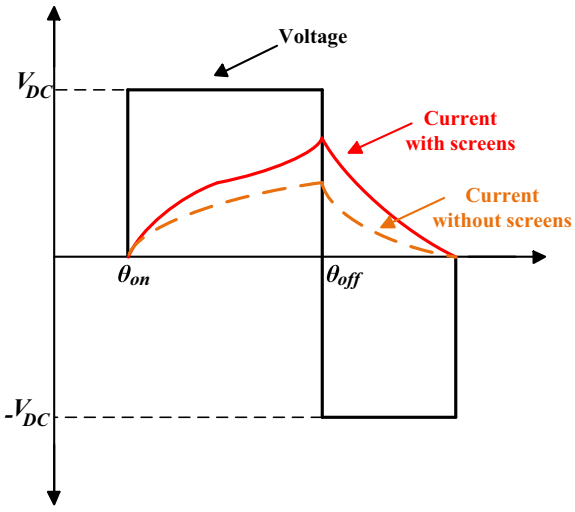


**FIGURE 3** Switched reluctance machine voltage and current waveforms with and without conducting screens

crossing through the rotor interpole region, unlike in Figure 4a. The reluctance path length $l$ is increased, and area $A$ is reduced, thus decreasing unaligned inductance $L$, since $L \propto A/l$.

## 3 | CALCULATION OF THE EFFECTIVE VALUE OF UNALIGNED INDUCTANCE USING THE FLUX TUBE METHOD

In the early design stage, it is time consuming to use the FEA to predict the motor performance [9]. Any change in the motor geometrical dimensions, number of stator/rotor poles, turns number, excitation current, or firing angles will dictate a new model to be built and simulated, involving a time-consuming process. Moreover, the SRM is heavily a non-linear machine. Then, scaling the design either up or down is not possible. Thus, suitable analytical methods are favoured for the initial design phase. Finally, the FEA could be used to fine-tune the design.

The flux linkage $\lambda$–current $i$ characteristics must be known at the aligned and unaligned positions to predict the motor performance. Generally, the conducting screens have a negligible effect on the aligned flux since the rotor pole arc is generally greater than the stator pole arc, so flux fringing and leakage are minimal. Nevertheless, the effective unaligned inductance is affected significantly.

In this section, the flux tube method [10] is used to calculate the effective unaligned inductance. Figure 5 shows the flux paths in the unaligned position, where five flux tubes are sufficient to describe the flux paths.

Figure 6 shows the equivalent magnetic circuit used to calculate the effective unaligned inductance, where, $R_{sp}$, $R_g$, $R_{rp}$, $R_{sy}$ and $R_{ry}$ are the reluctances for the stator pole, air gap, rotor pole, stator back iron, and rotor back iron, respectively. The different reluctances are calculated using machine geometrical dimensions.

Air gap reluctance dominates the unaligned reluctance resulting in linear flux linkage $\lambda-$current $i$ characteristics. Moreover, SRM phase winding is energised at an unaligned position. Hence, the current value at the unaligned position is small. Therefore, core saturation is not involved, which simplifies the analysis as opposed to the conventional flux tube approach that requires iterative solutions.

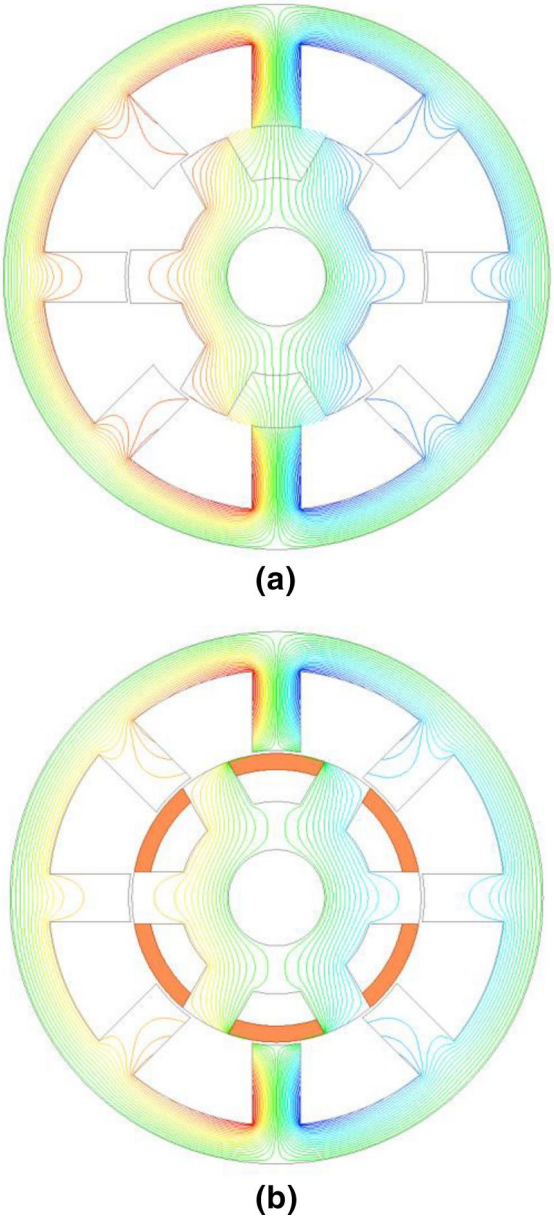


**FIGURE 4** Magnetic flux lines: (a) unscreened switched reluctance machine (SRM) and (b) screened SRM

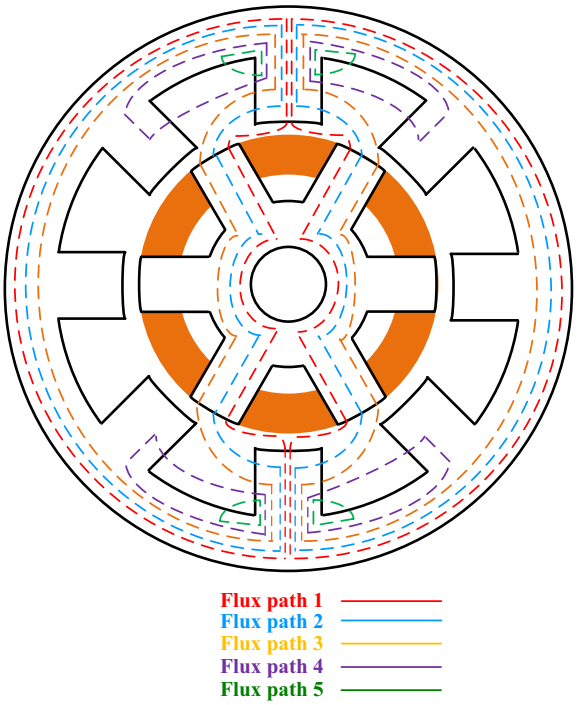


**FIGURE 5** Flux paths

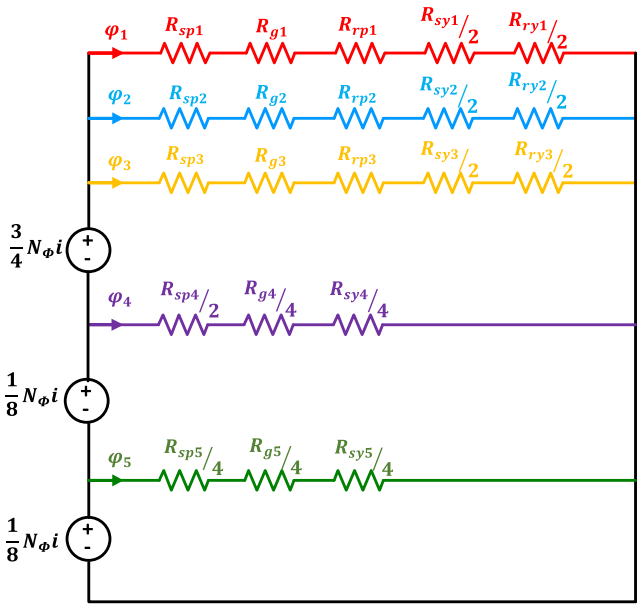


**FIGURE 6** Magnetic equivalent circuit

Generally, reluctance is defined by

$$R = l/\mu_0\mu_r A \tag{3}$$

where $l$ is the length of the flux path, $A$ is the cross-sectional area, and $\mu_0$ and $\mu_r$ are the permeability of air and Fe relative permeability, respectively. The reluctances for the five flux paths are formulated in the following subsections, where parameters $D_{sh}$, $d$, $D$ are the shaft diameter, rotor diameter, and outer stator diameter, respectively. $h_s$, $h_r$ are the stator and rotor pole heights, respectively. $b_{sy}$, $b_{ry}$ are the stator and rotor back iron, respectively. $\beta_s$, $\beta_r$ are the stator and rotor pole arcs, respectively. $\theta_s$, $\theta_r$ are the stator and rotor pole pitches, respectively $l_g$ is the air gap length, $L_s$ is the stack length, and $N_\Phi$ is the number of turns per phase.

## 3.1 | FLUX path #1

Figure 7 shows the flux path #1 with relevant angles required for derivation. The flux path involves the rotor back iron, the stator back iron, the rotor pole, the stator pole, and the air gap. Hence, five reluctances are used to complete the flux path. The flux path length and cross-sectional area are calculated as follows.

The flux is assumed to leave the stator pole at the tip and to enter the rotor pole at three-eighths$\beta_r$ from the pole tip.

### 3.1.1 | AIR gap reluctance, $R_{g1}$

The length of the air gap flux path is the arc $BC$, as shown in Figure 7, which is

$$length = BC = \tfrac{1}{2}(EB + EC)\theta_2^{rad} \tag{4}$$

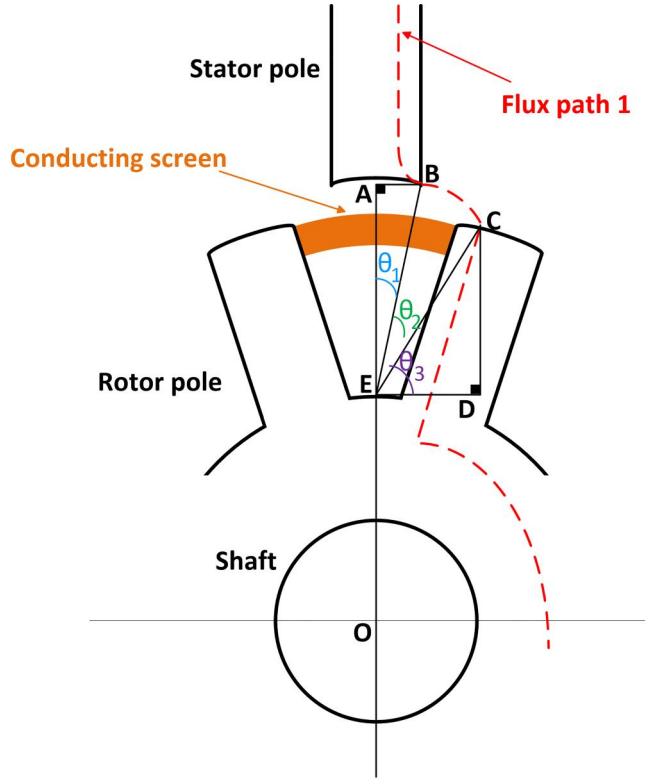


**FIGURE 7** Flux path #1

$EB$, $EC$ and $\theta_2$ are calculated using (5)-(7), respectively.

$$EB = \sqrt{AB^2 + AE^2} \tag{5}$$

$$EC = \sqrt{DC^2 + DE^2} \tag{6}$$

$$\theta_2^0 = 90^0 - \theta_1^0 - \theta_3^0 \tag{7}$$

The angles $\theta_1^0$ and $\theta_3^0$ are defined by (8) and (9), respectively.

$$\theta_1^0 = \tan^{-1} AB/AE \tag{8}$$

$$\theta_3^0 = \tan^{-1} DC/DE \tag{9}$$

The lengths $AB$, $AE$, $DC$, and $DE$ are given by (10)–(13), respectively.

$$AB = \tfrac{1}{2}d \sin \tfrac{1}{2}\beta_s \tag{10}$$

$$AE = \tfrac{1}{2}d \cos \tfrac{1}{2}\beta_s - \tfrac{1}{2}D_{sh} - b_{ry} \tag{11}$$

$$DC = \left(\tfrac{1}{2}d - l_g\right)\cos \tfrac{1}{2}(\theta_r - \tfrac{1}{4}\beta_r) - \tfrac{1}{2}D_{sh} - b_{ry} \tag{12}$$

$$DE = \left(\tfrac{1}{2}d - l_g\right)\sin\tfrac{1}{2}(\theta_r - \tfrac{1}{4}\beta_r) \tag{13}$$

The cross-sectional area is the average of the stator and rotor areas. The flux is confined to one-fourth $\beta_s$ of the stator pole arc and to one-fourth$\beta_r$ of the rotor pole arc. Hence, the area is defined as:

$$Area = \tfrac{1}{2}\left\{L_s\left(\tfrac{1}{8}d\beta_s^{rad}\right) + L_s\left(\tfrac{1}{2}d - l_g\right)\tfrac{1}{4}\beta_r^{rad}\right\} \tag{14}$$

### 3.1.2 | Stator pole reluctance, $\boldsymbol{R_{SP1}}$

The flux travels the length of the stator pole. Hence, the flux path's length is defined by (15), while the area is given by (16).

$$length = h_s \tag{15}$$

$$Area = \tfrac{1}{8}d\beta_s^{rad}L_s \tag{16}$$

### 3.1.3 | ROTOR pole reluctance, $\boldsymbol{R_{rP1}}$

Equation (17) defines the flux path's length in the rotor pole, representing the mean flux path. The area is given by (18):

$$length = h_r \tag{17}$$

$$Area = L_s\left(\tfrac{1}{2}d - l_g\right)\tfrac{1}{8}\beta_r^{rad} \tag{18}$$

### 3.1.4 | Stator back iron reluctance, $\boldsymbol{R_{sy1}}$

The flux path length in the stator back iron is defined by (19), while the area is given by (20):

$$length = \tfrac{1}{2}\pi\left\{D - b_{sy}\right\} \tag{19}$$

$$Area = L_s b_{sy} \tag{20}$$

### 3.1.5 | ROTOR back iron reluctance, $\boldsymbol{R_{ry1}}$

The flux path length in the rotor back iron is defined by (21), and the area is given by (22):

$$length = \tfrac{1}{2}\pi\left\{D_{sh} + b_{ry}\right\} \tag{21}$$

$$Area = L_s b_{ry} \tag{22}$$

After calculating the required reluctances, the inductance for flux path #1, $L_{u1}$ is

$$L_{u1} = \frac{(N_\Phi)^2}{R_{g1} + R_{sp1} + R_{rp1} + \tfrac{1}{2}R_{sy1} + \tfrac{1}{2}R_{ry1}} \tag{23}$$

## 3.2 | Flux path #2

The flux path #2 is illustrated in Figure 8, where the flux is assumed to leave the stator pole at one-fourth$h_s$ from the top of the stator pole and to enter the rotor pole in the middle.

### 3.2.1 | Air gap reluctance, $\boldsymbol{R_{g2}}$

The length of the air gap flux path is the arc $BC$, given by

$$length = BC = \tfrac{1}{2}(EB + EC)\theta_2^{rad} \tag{24}$$

$EB$, $EC$ and $\theta_2$ are calculated using (25)–(27), respectively.

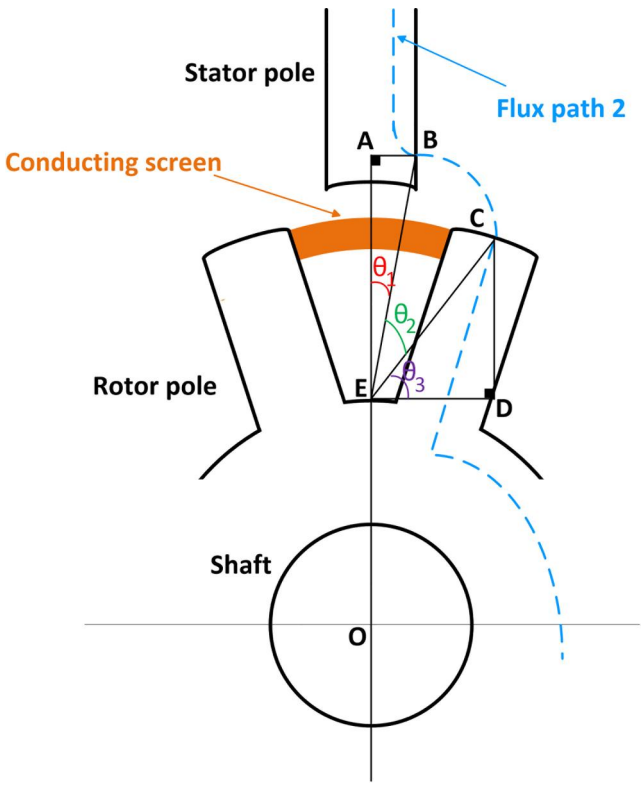


**FIGURE 8** Flux path #2

$$EB = \sqrt{AB^2 + AE^2} \tag{25}$$

$$EC = \sqrt{DC^2 + DE^2} \tag{26}$$

$$\theta_2^0 = 90^0 - \theta_1^0 - \theta_3^0 \tag{27}$$

The angles $\theta_1^0$ and $\theta_3^0$ are defined by (28) and (29), respectively:

$$\theta_1^0 = \tan^{-1} AB/AE \tag{28}$$

$$\theta_3^0 = \tan^{-1} DC/DE \tag{29}$$

The lengths *AB, AE, DC*, and *DE* are given by (30)–(33), respectively:

$$AB = \tfrac{1}{2} d \sin \tfrac{1}{2}\beta_s \tag{30}$$

$$AE = \tfrac{1}{2} d \cos \tfrac{1}{2}\beta_s + \tfrac{1}{4} h_s - \tfrac{1}{2} D_{sh} - b_{ry} \tag{31}$$

$$DC = \left(\tfrac{1}{2} d - l_g\right) \cos \tfrac{1}{2}\theta_r - \tfrac{1}{2} D_{sh} - b_{ry} \tag{32}$$

$$DE = \left(\tfrac{1}{2} d - l_g\right) \sin \tfrac{1}{2}\theta_r \tag{33}$$

The cross-sectional area is the average of the stator and rotor areas. The flux is confined to $\frac{1}{5}h_s$ of the stator pole height and to $\frac{1}{5}\beta_r$ of the rotor pole arc. Hence, the area is

$$Area = \tfrac{1}{2}\left\{ L_s\left(\tfrac{1}{5} h_s\right) + L_s\left(\tfrac{1}{2} d - l_g\right) \tfrac{1}{5} \beta_r^{rad} \right\} \tag{34}$$

### 3.2.2 | Stator pole reluctance, $\boldsymbol{R_{SP2}}$

The flux travels three-fourths$h_s$ of the stator pole, hence the length of the flux path is defined by (35), while the area is given by (36).

$$length = \tfrac{3}{4} h_s \tag{35}$$

$$Area = \tfrac{1}{5} h_s \, L_s \tag{36}$$

### 3.2.3 | Rotor pole reluctance, $\boldsymbol{R_{rP2}}$

Equation (37) defines the flux path's length in the rotor pole, representing the mean flux path. The area is given by (38):

$$length = h_r \tag{37}$$

$$Area = L_s\left(\tfrac{1}{2} d - l_g\right) \tfrac{1}{5} \beta_r^{rad} \tag{38}$$

### 3.2.4 | Stator back iron reluctance, $\boldsymbol{R_{sy2}}$

The length of the flux path in the stator back iron is defined by (39), while the area is given by (40):

$$length = \tfrac{1}{2}\pi\left\{ D - b_{sy} \right\} \tag{39}$$

$$Area = L_s b_{sy} \tag{40}$$

### 3.2.5 | Rotor back iron reluctance, $\boldsymbol{R_{ry2}}$

The length of the flux path in rotor back iron is defined by (41), and the area is given by (42):

$$length = \tfrac{1}{2}\pi\left\{ D_{sh} + b_{ry} \right\} \tag{41}$$

$$Area = L_s b_{ry} \tag{42}$$

Finally, the inductance for flux path #2, $L_{u2}$ is

$$L_{u2} = \frac{(N_\Phi)^2}{R_{g2} + R_{sp2} + R_{rp2} + \tfrac{1}{2} R_{sy2} + \tfrac{1}{2} R_{ry2}} \tag{43}$$

## 3.3 | FLUX path #3

Figure 9 shows the flux path #3, similar to the path #2, except for some different dimensions. The flux is assumed to leave the stator pole at three-fourths$h_s$, and to enter the rotor pole at five-eighths$\beta_r$ from the rotor pole tip.

### 3.3.1 | Air gap reluctance, $\boldsymbol{R_{g3}}$

The length of the air gap flux path is the arc *BC*, given by

$$length = BC = \tfrac{1}{2}(EB + EC)\theta_2^{rad} \tag{44}$$

*EB, EC* and $\theta_2$ are calculated using (45)–(47), respectively.

$$EB = \sqrt{AB^2 + AE^2} \tag{45}$$

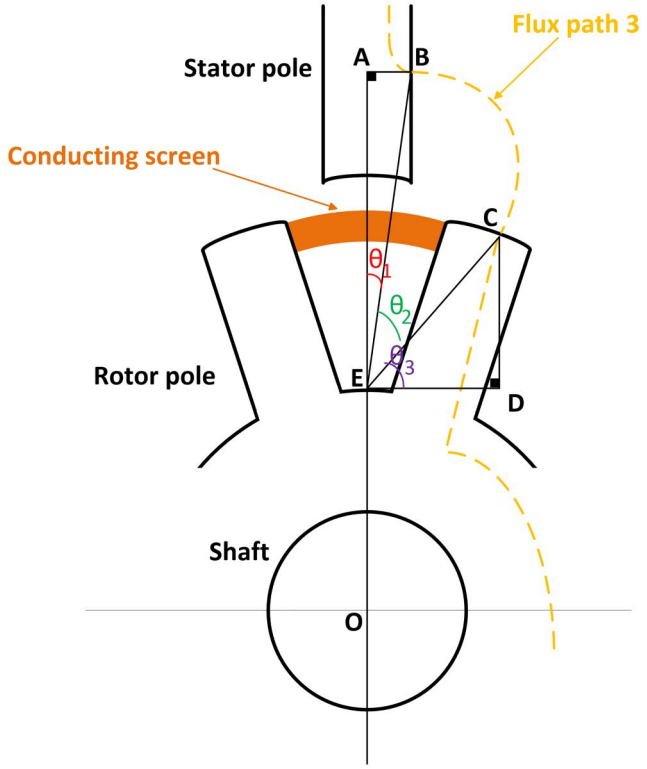


**FIGURE 9** Flux path #3

$$EC = \sqrt{DC^2 + DE^2} \tag{46}$$

$$\theta_2^0 = 90^0 - \theta_1^0 - \theta_3^0 \tag{47}$$

The angles $\theta_1^0$ and $\theta_3^0$ are defined by (48) and (49), respectively.

$$\theta_1^0 = \tan^{-1} AB/AE \tag{48}$$

$$\theta_3^0 = \tan^{-1} DC/DE \tag{49}$$

The lengths *AB*, *AE*, *DC*, and *DE* are given by (50)–(53), respectively.

$$AB = \tfrac{1}{2} d \sin \tfrac{1}{2}\beta_s \tag{50}$$

$$AE = \tfrac{1}{2} d \cos \tfrac{1}{2}\beta_s + \tfrac{3}{4} h_s - \tfrac{1}{2} D_{sh} - b_{ry} \tag{51}$$

$$DC = \left(\tfrac{1}{2} d - l_g\right) \cos \tfrac{1}{2}(\theta_r + \tfrac{1}{4}\beta_r) - \tfrac{1}{2} D_{sh} - b_{ry} \tag{52}$$

$$DE = \left(\tfrac{1}{2} d - l_g\right) \sin \tfrac{1}{2}(\theta_r + \tfrac{1}{4}\beta_r) \tag{53}$$

The cross-sectional area is the average of the stator and rotor areas. The flux is confined to one-fourth$h_s$ of the stator pole height and to one-fourth$\beta_r$ of the rotor pole arc. Hence, the area is

$$Area = \tfrac{1}{2}\left\{ L_s\left(\tfrac{1}{4} h_s\right) + L_s\left(\tfrac{1}{2} d - l_g\right) \tfrac{1}{4} \beta_r^{rad} \right\} \tag{54}$$

### 3.3.2 | Stator pole reluctance, $\boldsymbol{R_{SP3}}$

The flux travels only one-fourth$h_s$ of the stator pole, hence the length of the flux path is defined by (55), while the area is given by (56):

$$length = \tfrac{1}{4} h_s \tag{55}$$

$$Area = \tfrac{1}{4} h_s \, L_s \tag{56}$$

### 3.3.3 | Rotor pole reluctance, $\boldsymbol{R_{rP3}}$

Equation (57) defines the flux path's length in the rotor pole, representing the mean flux path. The area is defined by (58)

$$length = h_r \tag{57}$$

$$Area = L_s\left(\tfrac{1}{2} d - l_g\right) \tfrac{1}{4} \beta_r^{rad} \tag{58}$$

### 3.3.4 | Stator back iron reluctance, $\boldsymbol{R_{sy3}}$

The length of the flux path in the stator back iron is defined by (59), and the area is given by (60):

$$length = \tfrac{1}{2}\pi\left\{ D - b_{sy} \right\} \tag{59}$$

$$Area = L_s b_{sy} \tag{60}$$

### 3.3.5 | Rotor back iron reluctance, $\boldsymbol{R_{ry3}}$

The length of the flux path in rotor back iron is defined by (61), and the area is given by (62):

$$length = \tfrac{1}{2}\pi\left\{ D_{sh} + b_{ry} \right\} \tag{61}$$

$$Area = L_s b_{ry} \tag{62}$$

The inductance for flux path #3, $L_{u3}$ is

$$L_{u3} = \frac{(N_\Phi)^2}{R_{g3} + R_{sp3} + R_{rp3} + \tfrac{1}{2}R_{sy3} + \tfrac{1}{2}R_{ry3}} \quad (63)$$

## 3.4 | Flux path #4

The fourth flux path is shown in Figure 10. The flux flows from one stator pole to the adjacent stator pole through the air gap and returns via the stator back iron. The rotor is not involved in this flux tube. The three reluctances, $R_{g4}$, $R_{sp4}$, and $R_{sy4}$, for this flux tube are calculated as follows.

### 3.4.1 | AIR gap reluctance, $\boldsymbol{R_{g4}}$

The length of the air gap flux path is the arc $BC$:

$$length = BC = (OB)\theta_4^{rad} \quad (64)$$

$OB$ and $\theta_4$ are calculated using (65) and (66), respectively:

$$OB = \sqrt{AB^2 + AO^2} \quad (65)$$

$$\theta_4^0 = \theta_s - 2\theta_2^0 \quad (66)$$

where

$$AB = \tfrac{1}{2}d\sin\tfrac{1}{2}\beta_s \quad (67)$$

$$AO = \tfrac{1}{2}d\cos\tfrac{1}{2}\beta_s + \tfrac{1}{4}h_s \quad (68)$$

$$\theta_2^0 = \tan^{-1}AB/AO \quad (69)$$

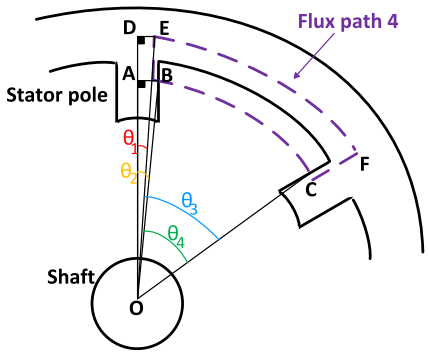


**FIGURE 10** Flux path #4

The cross-sectional area is given by

$$Area = \tfrac{1}{4}h_s L_s \quad (70)$$

### 3.4.2 | Stator pole reluctance, $\boldsymbol{R_{SP4}}$

The flux travels three-fourths$h_s$ of the stator pole. Hence, the length of the flux path is defined by (71), while the area is given by (72):

$$length = \tfrac{3}{4}h_s \quad (71)$$

$$Area = \tfrac{1}{4}h_s L_s \quad (72)$$

### 3.4.3 | Stator back iron reluctance, $\boldsymbol{R_{sy4}}$

The flux path length in the stator back iron is arc $EF$ defined by

$$length = EF = (OE)\theta_3^{rad} \quad (73)$$

OE and $\theta_3$ are calculated using (74) and (75), respectively:

$$OE = \sqrt{DE^2 + DO^2} \quad (74)$$

$$\theta_3^0 = \theta_s - 2\theta_1^0 \quad (75)$$

where

$$DE = \tfrac{1}{2}d\sin\tfrac{1}{2}\beta_s \quad (76)$$

$$DO = \tfrac{1}{2}d\cos\tfrac{1}{2}\beta_s + h_s + \tfrac{1}{4}b_{sy} \quad (77)$$

$$\theta_1^0 = \tan^{-1}DE/DO \quad (78)$$

The cross-sectional area is given by

$$Area = L_s b_{sy} \quad (79)$$

The flux is assumed to link only one-fourth of the number of turns per phase ($N_\Phi$). Hence, the inductance for the flux path #4, $L_{u4}$ is calculated using

$$L_{u4} = \frac{(\tfrac{1}{4})^2(N_\Phi)^2}{\tfrac{1}{2}R_{sp4} + \tfrac{1}{4}R_{g4} + \tfrac{1}{4}R_{sy4}} \quad (80)$$

### 3.5 | Flux path #5

The last flux path is illustrated in Figure 11. The flux leaves the stator pole to enter the stator back iron, passing through the air gap. The flux path is assumed to represent the perimeter of a quarter circle with centre at point A and radius of a quarter the stator pole height one-fourth$h_s$. The reluctances are calculated as follows.

#### 3.5.1 | AIR gap reluctance, $\boldsymbol{R_{g5}}$

The length of the air gap flux path is defined by (81), representing the length of arc BC. The area is given by (82):

$$length = ½\pi \times ¼h_s \tag{81}$$

$$Area = \ ⅛h_s\, L_s \tag{82}$$

#### 3.5.2 | Stator pole reluctance, $\boldsymbol{R_{SP5}}$

The length of the flux path in the stator pole is defined by (83), and the area is given by (84):

$$length = ¼\left(h_s + b_{sy}\right) \tag{83}$$

$$Area = \ ⅛h_s L_s \tag{84}$$

#### 3.5.3 | Stator back iron reluctance, $\boldsymbol{R_{sy4}}$

The flux path length in the stator back iron is defined by (85), where the area is given by (86):

$$length = ¼h_s \tag{85}$$

$$Area = \ L_s b_{sy} \tag{86}$$

The flux is assumed to link only one-eighth the turns per phase ($N_\Phi$), hence the inductance for the flux path #5, $L_{u5}$ is

$$L_{u5} = \frac{(⅛)^2 (N_\Phi\ )^2}{¼R_{sp5} + ¼R_{g5} + ¼R_{sy5}} \tag{87}$$

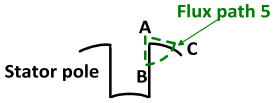


**FIGURE 11** Flux path #5

Finally, the effective unaligned inductance is the sum of the unaligned inductances for the five flux tubes, calculated using

$$L_{ueff} = \sum_{k=1}^{5} L_{uk} \tag{88}$$

## 4 | VALIDATION

Static FEA, which is a widely accepted toolbox for assessing machine design [11,12] is used to validate the proposed flux tube method for calculating the effective unaligned inductance of SRM with conducting screens. The proposed method is validated using four different SRMs, with specifications given in Table 1.

Table 2 compares the value of unaligned inductances obtained using mathematical calculations (as proposed in the previous section) with the values obtained using 2D and 3D FEA.

A step voltage is applied on the phase winding in the static FEA, hence $d\varphi/dt$ is established, and the effect of the screen is observed. Otherwise, if a constant DC voltage is applied to

**TABLE 1** SRM specifications

| Parameter | Value | Value | Value | Value |
|---|---|---|---|---|
| No. of motor phases $m$ | 4 | 3 | 4 | 3 |
| Stator/rotor poles $N_s/N_r$ | 8/6 | 6/4 | 8/6 | 6/4 |
| Turns per pole $N$ | 90 | 125 | 77 | 268 |
| Stack length | 155 mm | 100 mm | 200 mm | 60.37 mm |
| Shaft radius | 15 mm | 15 mm | 14 mm | 14 mm |
| Rotor outer radius | 45 mm | 50 mm | 49.8 mm | 51.03 mm |
| Thickness of rotor yoke | 15 mm | 15 mm | 16 mm | 10.5 mm |
| Rotor pole arc | 21° | 36° | 21.6° | 36° |
| Stator inner radius | 46 mm | 50.5 mm | 50.3 mm | 51.28 mm |
| Stator outer radius | 83 mm | 90 mm | 95 mm | 95 mm |
| Thickness of stator yoke | 12 mm | 14.5 mm | 12 mm | 10.5 mm |
| Stator pole arc | 18.9° | 30° | 18° | 24° |

**TABLE 2** Unaligned inductance values

| | SRM-1 | SRM-2 | SRM-3 | SRM-4 |
|---|---|---|---|---|
| Proposed method (mH) | 4.66 | 5.95 | 4.62 | 14.9 |
| FEA-2D (mH) | 4.87 | 5.55 | 4.74 | 13.46 |
| % Error | - 4.3% | +7.2% | - 2.5% | +10.7% |
| FEA-3D (mH) | 5.16 | 6.1 | 4.93 | 15.6 |
| % Error | −9.7% | −2.5% | −6.3% | −4.5% |

the phase winding, there will be no rate of change of flux, and the screen will not be exploited.

The good engineering correlation between the analytical and the static FEA values validates the proposed flux tube method. In SRMs with short stack length, as with SRM-2 and SRM-4, the effect of coil end winding, and the value of leakage flux is not insignificant at an unaligned position [13]. 3D FEA accounts for the leakage flux; hence 3D FEA results are more accurate than 2D FEA for short stack length SRMs.

## 5 | DESIGN AND PERFORMANCE OF SRM WITH ROTOR CONDUCTING SCREENS

In this section, the design and dynamic performance of SRM with rotor conducting screens are investigated.

### 5.1 | SRM design

It has to be noted that the SRM design is not a straight forward task. The double salient structure increases the saturation effect in the pole tips. Fringing is not insignificant. The design process starts by initialising the machine dimensions using analytical formulas. FEA is then used to fine-tune the initial design.

#### 5.1.1 | Selecting the number of phases and poles

The first step in the SRM design is to choose the number of phases, stator poles, and rotor poles [14]. The selection is generally based on the application. For instance, in low-cost high-speed applications, where performance could be sacrificed in favour of cost, like small home appliances, usually a single-phase or a two-phase SRM is selected. The single-phase SRM cannot inherently and reliably self-start. Increasing the number of SRM phases reduces the torque ripple, improves the fault tolerance capability, and improves SRM performance, at the expense of converter costs.

The switching frequency for a phase of the SRM is calculated using (89)

$$f_{sw} = \frac{\omega}{2\pi} N_r \tag{89}$$

Considering (89), if the number of rotor poles is increased (while keeping the number of phases unchanged) [15], torque ripple will be reduced, and an economical converter could be used. Coil end winding will be smaller, allowing increased stack length while maintaining the overall machine axial length unchanged. Hence, torque density will be improved, but the switching frequency will increase, resulting in higher core losses.

If the number of rotor poles is increased (while keeping the number of stator poles unchanged) [16], the interpolar rotor air gaps will be narrower. Hence, the unaligned inductance will be significantly higher than that of the conventional SRM. The unaligned inductance increase will reduce the energy conversion area, thus decreasing the developed torque. Additionally, the current rise time at phase turn on is prolonged due to higher unaligned inductance, which implies using higher dc-link voltages to increase the current rate of rise.

A $4\varphi$ ($m = 4$) 8/6 ($N_s/N_r$) SRM is selected. An asymmetric half-bridge with two switches and two diodes per phase is used to assess the SRM performance.

#### 5.1.2 | Sizing stack length, stator and rotor diameters, and air gap length

The output torque is defined by (90)

$$T_e = KL_s d^2 \tag{90}$$

where K is a constant in the range of 10.3 to 34.5 kNm/m3 representing the product of electrical and magnetic loading of the SRM. Using (90) and for the required output torque, the product of the stack length and the square of the rotor diameter is known. A 1∼3 ratio between the stack length and rotor diameter $L_s/d$ is advised in [17] for servo applications. Hence, the rotor outer diameter is selected to be 90 mm, while the stack length is 157.5 mm for 26N.m output torque.

The ratio between the stator diameter and rotor diameter $D/d$ is $1.5 \sim 1.8$. Thus, the stator diameter is selected to be 162 mm.

Reducing the SRM air gap increases the torque density of the SRM. A typical SRM air gap length for SRM is between 0.25 and 1 mm, where a 1 mm air gap length is selected.

#### 5.1.3 | Sizing stator and rotor pole arcs

Selecting adequate stator and rotor pole arcs is of prime importance. Miscalculations could lead to self-starting problems. Hence, to assure torque production at all rotor positions, the stator pole arc is calculated using (91).

$$\beta_s \geq \frac{2\pi}{mN_r} \tag{91}$$

Usually, the stator pole arc is selected slightly smaller than the rotor pole arc to allow more stator slot area to accommodate the winding. For a complete unaligned position to be achieved, (92) should be satisfied.

$$\beta_s + \beta_r < \frac{2\pi}{N_r} \tag{92}$$

The selected stator and rotor pole arcs are $18.9^0$ and $21^0$, respectively.

### 5.1.4 | Sizing stator and rotor back iron widths and pole heights

Large stator back iron is desirable to reduce vibration, increase mechanical strength, and ease saturation [18]. However, an excessively large value will reduce the available space for stator winding. The rotor back iron has the same constraint as the stator back iron regarding saturation. The rotor pole height should be several times larger than the air gap to increase the conversion area (reducing the unaligned inductance). Hence, (93) gives an initial value for the stator and rotor pole heights and back iron, respectively.

$$h_s,\ h_r,\ b_{sy}, b_{ry} > \frac{d}{2}\sin\beta_r/2 \tag{93}$$

The stator and rotor pole heights and back iron are 25 , 15, 10, and 15 mm, respectively.

### 5.1.5 | Estimating rms current, and current density

Determining SRM current density is of prime importance as it is related to the cooling method adopted. The rms current is defined by (94).

$$I_{rms} = \frac{P}{\sqrt{m}n\eta k_d V_{DC}} \tag{94}$$

where P is the motor output power ($T_e X\omega$), n is the number of phases conducting simultaneously, $\eta$ is the motor efficiency, and $k_d$ is the SRM duty cycle.

For 420 V dc-link voltage, 26 N·m output power, 1800 rpm, the rms current is 13 A.

The current density is directly related to the phase rms current using (95).

$$J_{rms} = \frac{NI_{rms}}{k_s A_s/2} \tag{95}$$

where $N$ is the number of turns per pole, $A_s$ is the slot area and $k_s$ is the slot fill factor (ratio between copper winding and slot areas).

The slot fill factor depends on the conductor shape and the slot form. Increasing the value of $k_s$ is desirable to reduce the current density. The slot fill factor is low (40%), if loosely bundled conductors are used. This value increases to 60%, if rectangular conductors are used. Finally, the slot fill factor could be improved to reach 80%, if the conductors are customised to fit the slot shape.

If the SRM is designed to be totally enclosed, then the current density should not exceed 5 A/$mm^2$. This value increases to 10 A/$mm^2$ for fan cooling, and with liquid cooling, the current density should be less than 30 A/$mm^2$.

The slot area in the designed SRM is 770$mm^2$. With a 0.5 slot fill factor and 90 turns per pole, the current density is 6 A/$mm^2$.

## 5.2 | Static performance of the designed SRM

Figure 12 shows the flux linkage–current ($\lambda$–$i$) characteristics at unaligned and aligned positions for the designed SRM. While Figure 13 shows the static torque profile at different current levels.

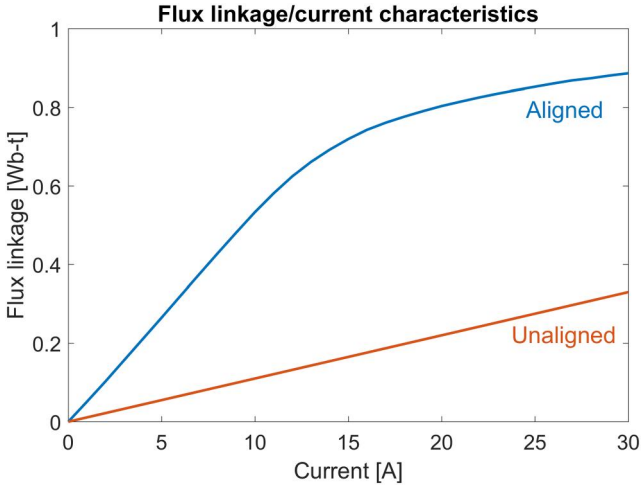


**FIGURE 12** Flux linkage/current characteristics

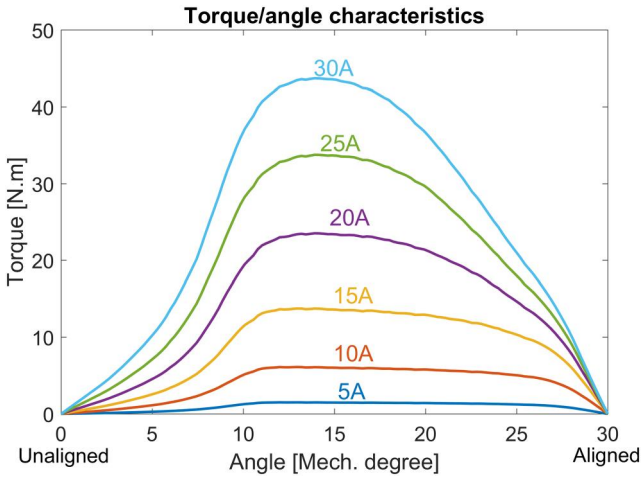


**FIGURE 13** Static torque characteristics

### 5.3 | SRM performance with rotor conducting screens

In this subsection, the performance of SRM without and with rotor conducting screens are compared.

Table 3 shows the value of unaligned inductance along with the increase in magnetic co-energy when rotor conducting screens are deployed. The unaligned inductance without rotor conducting screens is 11.14 mH. This value drops to 5.3mH when conducting screens are used. A 20% increase in the magnetic co-energy is observed, which reflects on the developed torque.

In addition, the rms current (and thereby current density) is expected to increase when rotor conducting screens are deployed due to the reduction in unaligned inductance. According to (94) and (95), the rms current is predicted to be 15.6 with 7.3 A/mm$^2$ current density.

Figure 14 compares the performance of the unscreened and the screened SRM. Both SRMs operate at base speed (1800 rpm) with $\theta_{on} = 30^0$ and $\theta_{off} = 47.3^0$. At the base speed, the SRM back emf equals the dc-link voltage. Hence the SRM operates in single-pulse mode. The unmodified SRM delivers a rated load, 26 Nm, 4.9 kW.

Figure 14a shows that the reduction in the effective unaligned inductance allows the current in the phase winding to build up quicker for the screened SRM than for the unscreened machine. The rms phase current increases from 12.52 A in the unscreened SRM to 15.25 A in the screened SRM (close to the predicted value).

Figure 14b illustrates that the increase in the phase winding current reflects on the developed torque, where a 19.5% increase in the developed torque is recorded.

Unfortunately, rotor conducting screens are associated with heavy eddy current losses, as illustrated in Figure 15, reducing the efficiency of the SRM.

Table 4 compares the SRM performance without and with the rotor conducting screens.

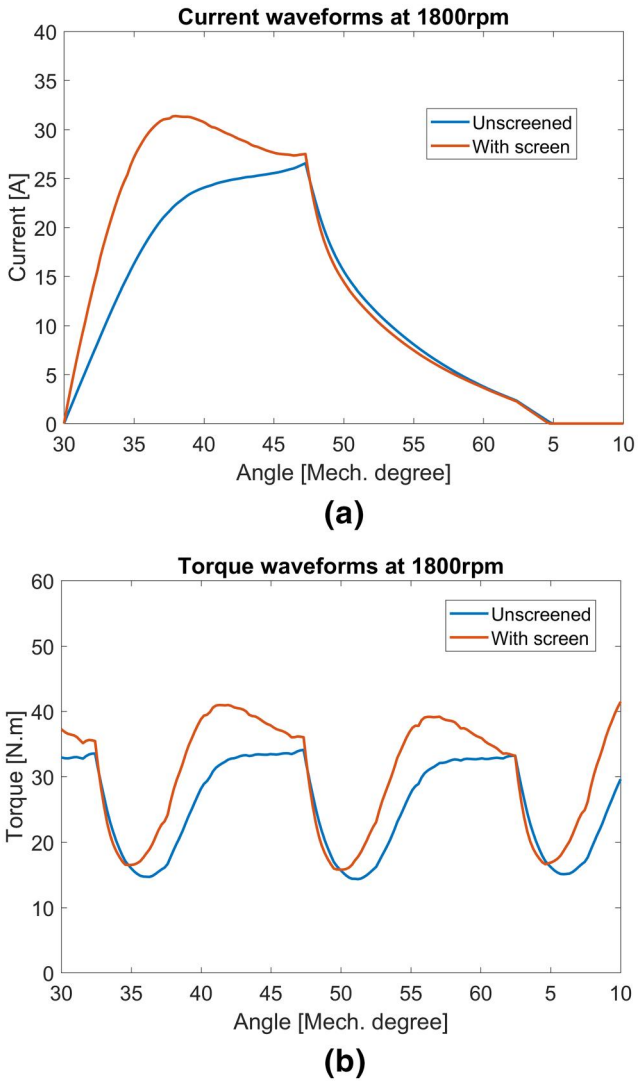


**FIGURE 14** Switched reluctance machine without and with rotor conducting screens performance at 1800 rpm: (a) current waveforms, and (b) torque waveforms

## 6 | ACOUSTIC NOISE AND TORQUE RIPPLE REDUCTION

SRM electromagnetic attraction forces are divided into two components, namely, tangential and radial components. The former is directly related to the developed torque of the machine. That is, maximising this component is one of the goals while designing the SRM, but the radial component does not contribute to the process of rotational torque

**TABLE 3** Unaligned inductance values and increase in co-energy for screened SRM

| | Proposed | 2D-FEA | 3D-FEA |
|---|---|---|---|
| Unaligned inductance (mH) | 4.83 | 5 | 5.3 |
| Increase in co-energy (%) | 21.6 | 21 | 20 |

Abbreviation: SRM, switched reluctance machine.

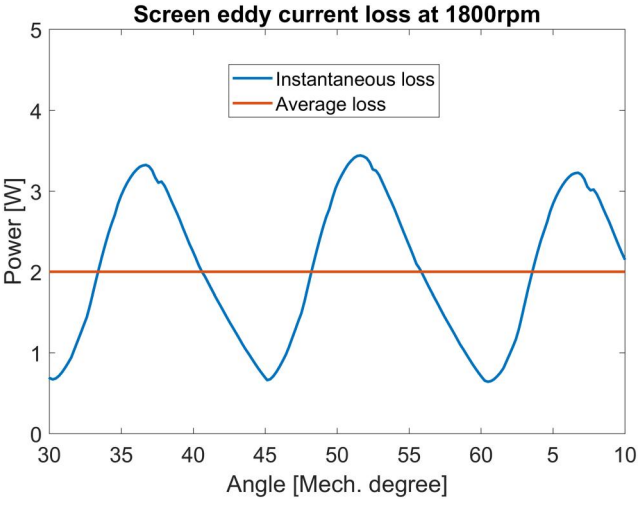


**FIGURE 15** Screen eddy current loss at 1800 rpm

**TABLE 4** Comparison between switched reluctance machine without and with rotor conducting screens

| Parameter | Unmodified SRM | SRM with rotor conducting Screens |
|---|---|---|
| Unaligned inductance (mH) | 11.14 | 5.3 |
| DC link voltage (V) | 420 | 420 |
| Base speed (rpm) | 1800 | 1800 |
| Output torque (Nm) | 26 | 31 |
| Output power (kW) | 4.9 | 5.85 |
| Rms current (A) | 12.52 | 15.25 |
| Current density (A/mm$^2$) | 5.85 | 7.13 |
| Efficiency at base speed (%) | 93 | 71 |
| Torque ripple (%) | 73 | 74 |

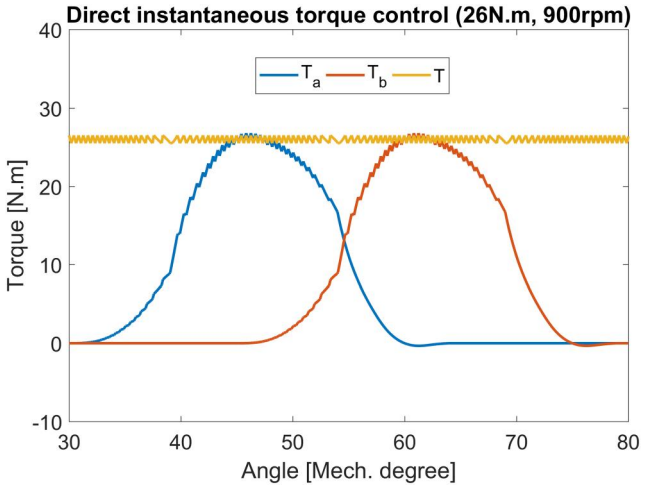


**FIGURE 16** Direct instantaneous torque control at 26 Nm and 900 rpm

production. It is the main reason for vibration, stator deformation, and acoustic noise. Hence, eliminating or minimising this component will improve the SRM performance. It is shown in [19] that skewing the stator and the rotor of a three-phase 12/8 SRM reduces vibration and acoustic noise. A simple solution proposed in [20] uses stator spacers, which are non-magnetic materials such as ceramics inserted between the stator poles, to reduce stator vibration and thereby the acoustic noise.

The problem of rotational torque ripple (TR) arises due to the discrete nature of torque production. Although the deployment of rotor conducting screens does not significantly alter the torque ripple value, the TR minimisation technique should be adopted for satisfactory operation.

Several TR minimisation approaches are available as torque sharing functions, current profiling, and direct instantaneous torque control (DITC) [21]. The DITC approach results at 26N.m and 900rpm are illustrated in Figure 16, where less than 4% TR is recorded. Hence, satisfactory operation of the SRM is achieved.

## 7 | CONCLUSION

This article investigated the effect of utilising rotor conducting screens to decrease SRM effective unaligned inductance, thus increasing the conversion area and thereby the developed torque. The prediction of SRM performance is based on knowing the magnetic characteristics at unaligned and aligned positions. Hence, based on the flux tube method, a detailed analytical method is proposed to calculate the effective unaligned inductance for a screened SRM. The proposed method was assessed on four different SRMs (two 3φ SRMS and two 4φ SRMs), where acceptable agreement between the proposed method and the FEA was recorded. A detailed design procedure for initialising SRM with rotor conducting screens is presented.

## CONFLICT OF INTEREST

All authors acknowledge and confirm that there is no conflict of interest to disclose.

## ORCID

*Aly A. Abdel-Aziz* https://orcid.org/0000-0003-1681-7966

## REFERENCES

1. Kiyota, K., Nakano, S., Chiba, A.: A fast calculation method of optimal ratio of outer diameter and axial length for torque improvement in switched reluctance motor. IEEE Trans. on Ind. Appl. 54(6), 5802–5811 (2018)
2. Hutton, A., Miller, T.: Use of flux screens in switched reluctance motors. In: IEEE 4th International Conference on Electrical Machines and Drives, London, UK, pp. 312–316 (1989)
3. Dessouky, Y.G., Williams, B.W., Fletcher, J.E.: Conducting screen utilisation in switched reluctance motors. IEEE Trans. Energy Conv. 14(4), 946–951 (1999)
4. Hamdy, R., et al.: High-speed performance improvements of a two-phase switched reluctance machine utilising rotor-conducting screens. IEEE Trans. Energy Conv. 17(4), 500–506 (2002)
5. Mahmoud, M., Fletcher, J., Williams, B.: Evaluation of rotor conducting screens on the rotor of the single-phase switched reluctance machine. In: IEEE 2nd International Conference on Power Electronics, Machines and Drives, Edinburgh, UK, pp. 18–23 (2004)
6. Lovatt, H.C.: Analytical model of a classical switched-reluctance motor. IEE Proc. Electr. Power Appl. 152(2), 352–358 (2005)

7. Kokernak, J.M., Torrey, D.A.: Magnetic circuit model for the mutually coupled switched-reluctance machine. IEEE Trans. Magn. 36(2), 500–507 (2000)
8. Materu, P., Krishnan, R.: Analytical prediction of SRM inductance profile and steady-state average torque. In: IEEE Industry Applications Society Annual Meeting, Seattle, USA, pp. 214–223 (1990)
9. Sheth, N.K., Rajagopal, K.R.: Calculation of the flux-linkage characteristics of a switched reluctance motor by flux tube method. IEEE Trans. Magn. 41(10), 4069–4071 (2005)
10. Krishnan, R.: Switched Reluctance Motor Drives: Modelling, Simulation, Analysis, Design and Applications. CRC Press, Boca Raton, FL (2001)
11. Jiang, J.W., Bilgin, B., Emadi, A.: Three-phase 24/16 switched reluctance machine for a hybrid electric powertrain. IEEE Trans. Transp. Electrif. 3(1), 76–85 (2017)
12. Diao, K., et al.: Multiobjective system level optimization method for switched reluctance motor drive systems using finite-element model. IEEE Trans. Ind. Electron. 67(12), 10055–10064 (2020)
13. Lin, J., Schofield, N., Emadi, A.: External-rotor $6-10$ switched reluctance motor for an electric bicycle. IEEE Trans. Transp. Electrif. 1(4), 348–356 (2015)
14. Chau, K.: Switched reluctance motor drives. In: Electric Vehicle Machines and Drives: Design, Analysis and Application, pp. 108–146. IEEE (2015)
15. Chiba, A., et al.: Torque density and efficiency improvements of a switched reluctance motor without rare-earth material for hybrid vehicles. IEEE Trans. Ind. Appl. 47(3), 1240–1246 (2011)
16. Desai, P.C., et al.: Novel switched reluctance machine configuration with higher number of rotor poles than stator poles: concept to implementation. IEEE Trans. Ind. Electron. 57(2), 649–659 (2010)
17. Krishnan, R., Arumugan, R., Lindsay, J.F.: Design procedure for switched-reluctance motors. IEEE Trans. Ind. Appl. 24(3), 456–461 (1988)
18. Kiyota, K., Chiba, A.: Design of switched reluctance motor competitive to 60-kW IPMSM in third-generation hybrid electric vehicle. IEEE Trans. Ind. Appl. 48(6), 2303–2309 (2012)
19. Gan, C., et al.: Investigation of skewing effects on the vibration reduction of three-phase switched reluctance motors. IEEE Trans. Magn. 51(9), 1–9 (2015)
20. Rasmussen, P.O., Andreasen, J.H., Pijanowski, J.M.: Structural stator spacers-a solution for noise reduction of switched reluctance motors. IEEE Trans. Ind. Appl. 40(2), 574–581 (2004)
21. Gan, C., et al.: A review on machine topologies and control techniques for low-noise switched reluctance motors in electric vehicle applications. IEEE Access. 6, 31430–31443 (2018)


**How to cite this article:** Abdel-Aziz, A.A., et al.: Unaligned inductance calculation using flux tube approach for rotor conducting screen-based SRM. IET Electr. Power Appl. 15(8), 1081–1094 (2021). https://doi.org/